Supporting Information

Tumor-targeting Semi-rigid Metal-organic-polymer Framework Nanoparticles with High Adaptability and Bioavailability

Shuxuan Liu[1, 2, §], Kaiteng Pang[3, §], Meili Sun[4, §], Jie Qiao[1, 2], Hongjing He[1,2], Yao Wang[1, 2], Liqiong Liao[3, *], Hao Li[1, 2, *], and Guofu Zhou[1, 2]

[1] Guangdong Provincial Key Laboratory of Optical Information Materials and Technology, Institute of Electronic Paper Displays, South China Academy of Advanced Optoelectronics, South China Normal University, Guangzhou 510006, P. R. China

[2] National Center for International Research on Green Optoelectronics, South China Normal University, Guangzhou 510006, P. R. China

[3] Biomaterials Research Center, School of Biomedical Engineering, Southern Medical University, Guangzhou 510515, P.R. China

[4] Department of Radiology, Sun Yat-sen University Cancer Center, State Key Laboratory of Oncology in South China, Collaborative Innovation Center for Cancer Medicine, Sun Yat-sen University, Guangzhou 510050, P. R. China

* Correspondence should be addressed to:

Professor Hao Li; Tel: +86-20-39314813; Fax: +86-20-39314813

E-mail: haoli@m.scnu.edu.cn

Professor Liqiong Liao; E-mail: liqiongliao@hotmail.com

[§]These authors contributed equally to this work.

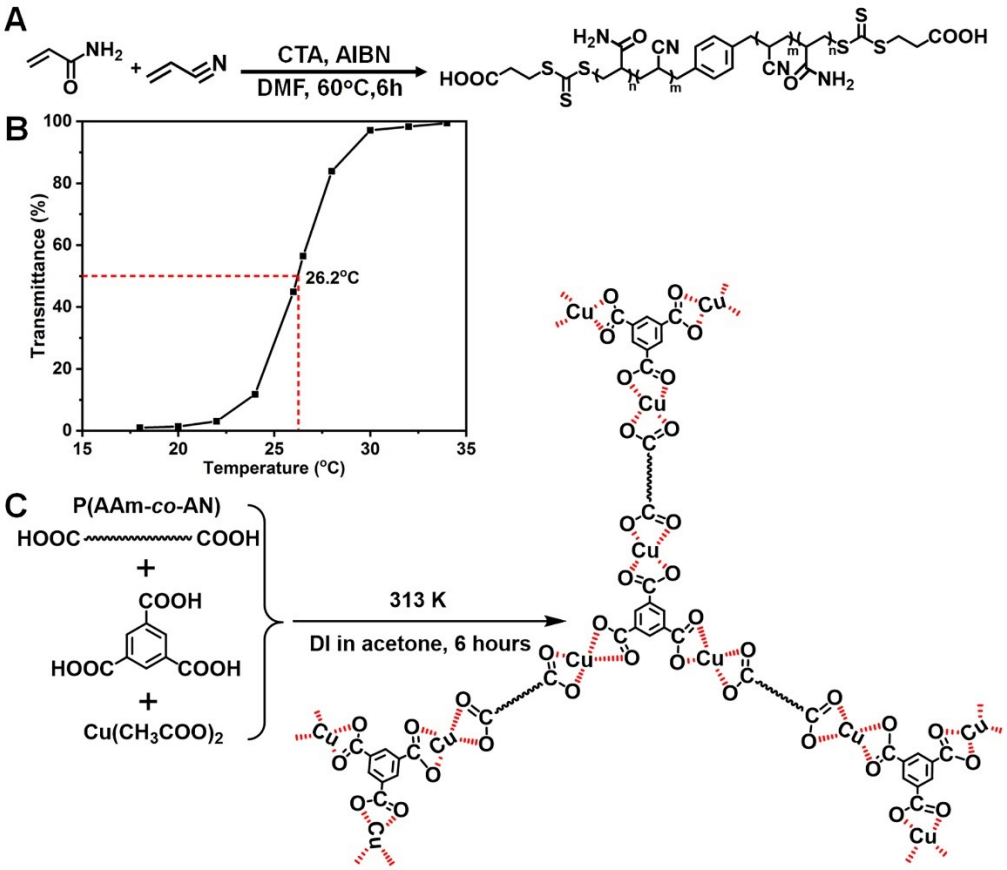

Figure S1 (A) Synthetic route of random P(AAm-*co*-AN) copolymer; (B) turbidity profile of the resulting P(AAm-co-AN) copolymer; (C) synthetic route of MOPF.

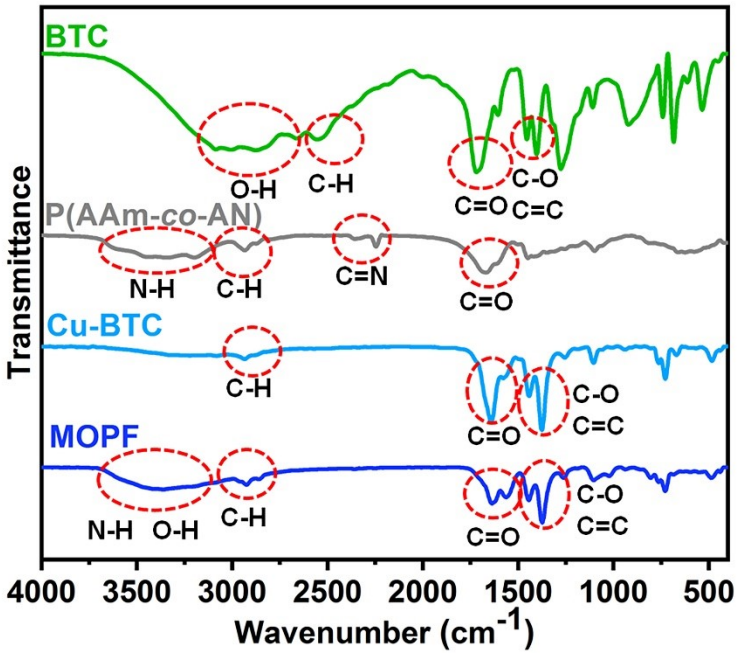

Figure S2 FT-IR spectra of BTC, P(AAm-*co*-AN) copolymer, Cu-BTC MOF, and resulting MOPF nanoparticles.

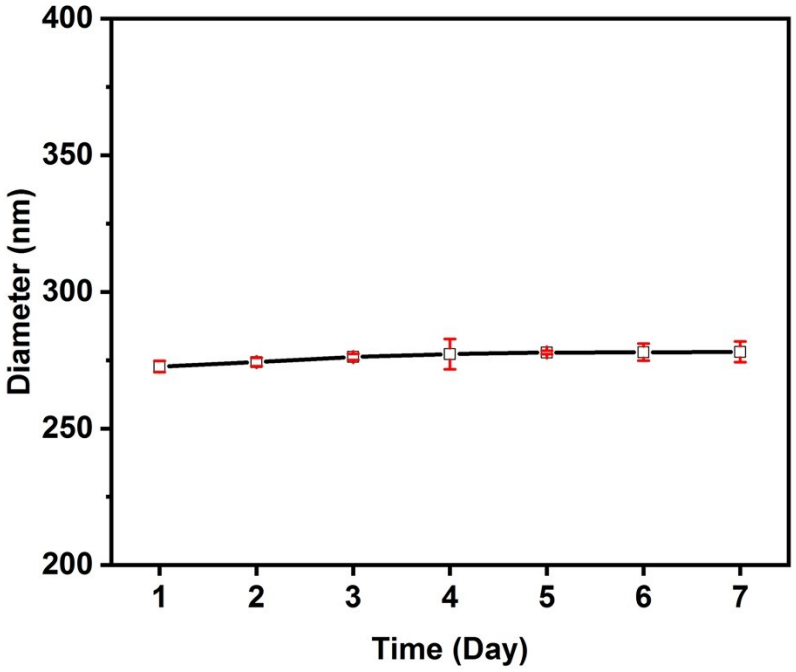

Figure S3. Particle sizing variation of the resulting MOPF nanoparticle within a week.

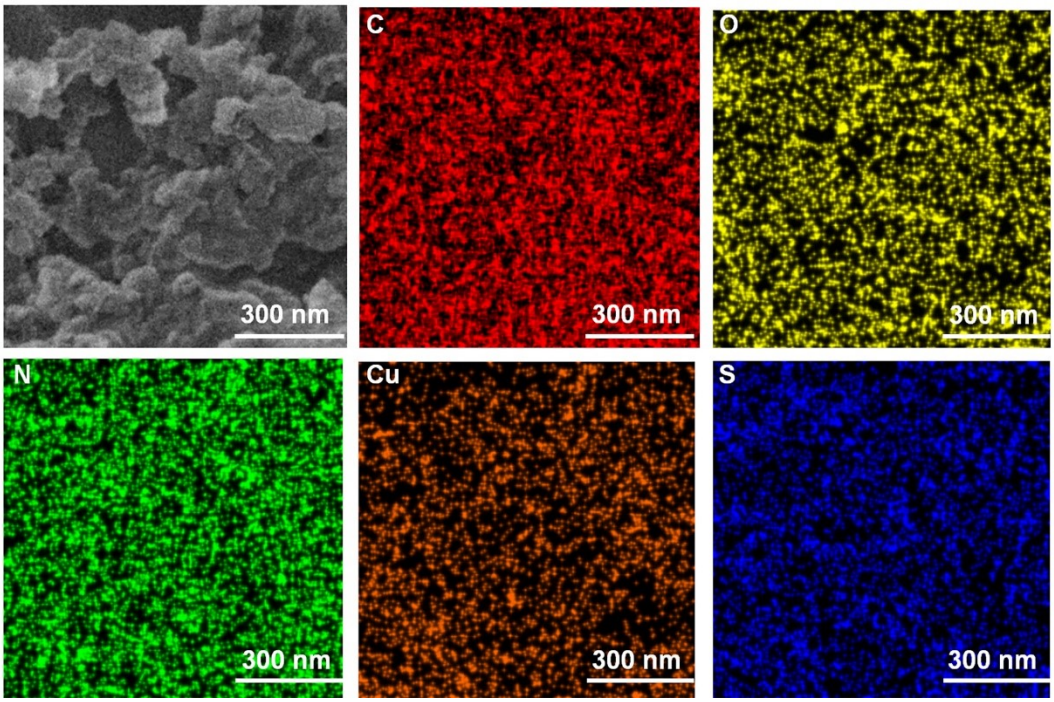

Figure S4. EDS elemental mappings of the resulting MOPF nanoparticles.

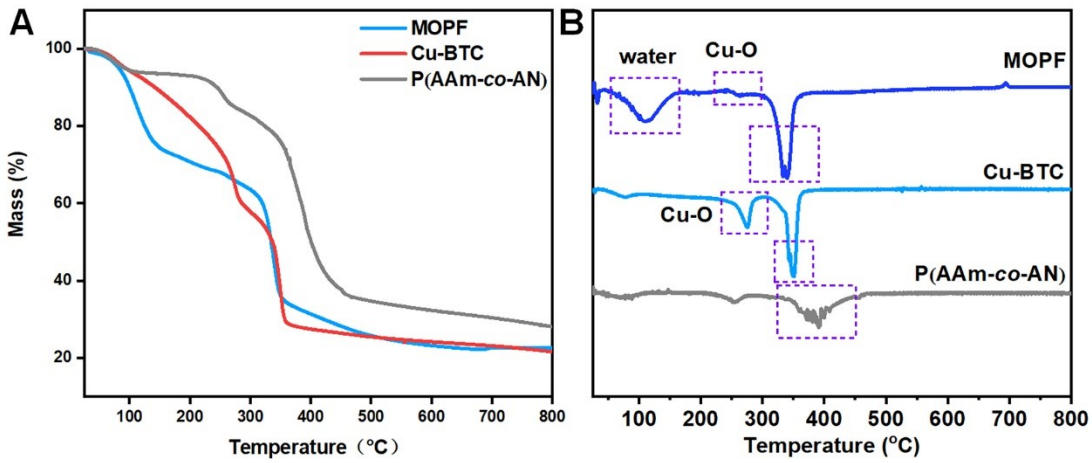

Figure S5. (A) TGA curves and (B) the corresponding differential thermogravimetric (DTG) curves of the resulting P(AAm-co-AN) copolymer, Cu-BTC MOF, and MOPF nanoparticles.

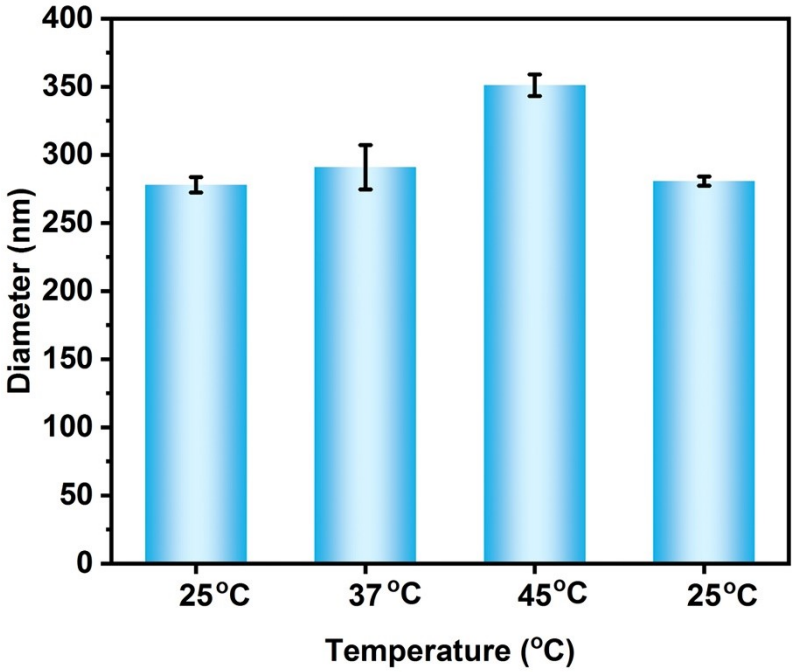

Figure S6. Particle sizing variations of the resulting MOPF nanoparticles in deionized water (concentration: 0.05 mg/mL) at different temperatures.

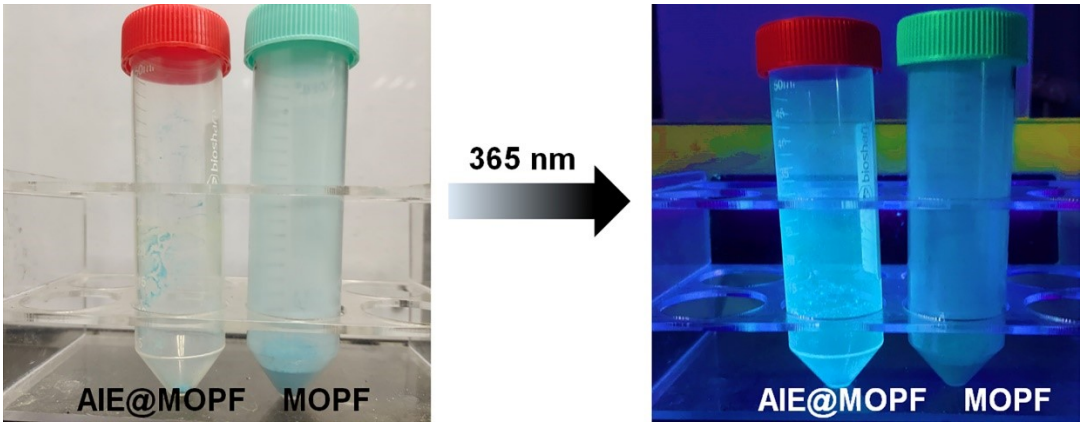

Figure S7. Blank and TPE-loaded MOPF nanoparticles (AIE@MOPF) before and after UV irradiation (365 nm).

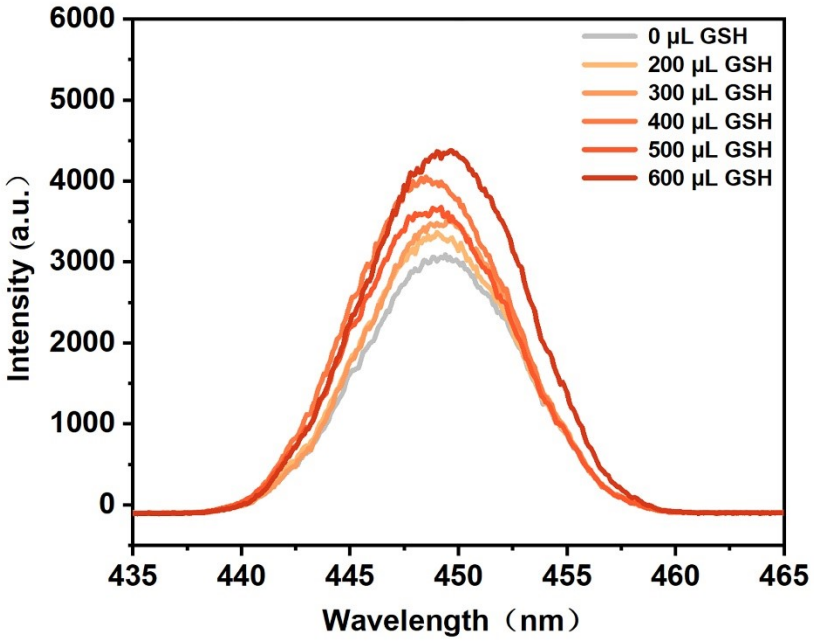

Figure S8. Fluorescence spectra of the aqueous MOPF solution (concentration: 1000 mg/mL) after adding different volume of aqueous GSH solution (concentration: 5 mM) and aqueous DTNB solution (concentration: 5 mM) in turn in the wavelength range between 435 and 465 nm.

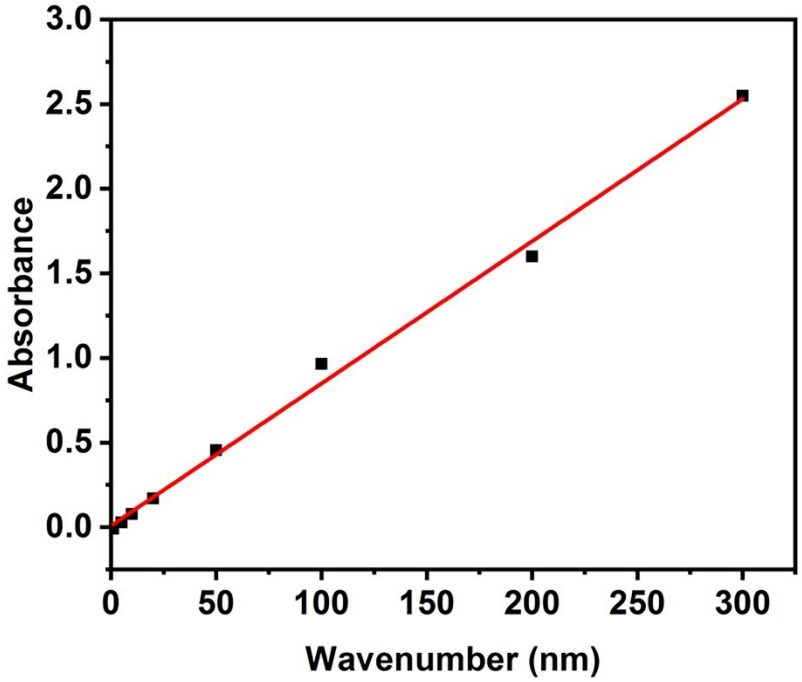

Figure S9. Standard absorbance-concentration curve of lenalidomide (LE) in ethyl acetate at 306 nm.

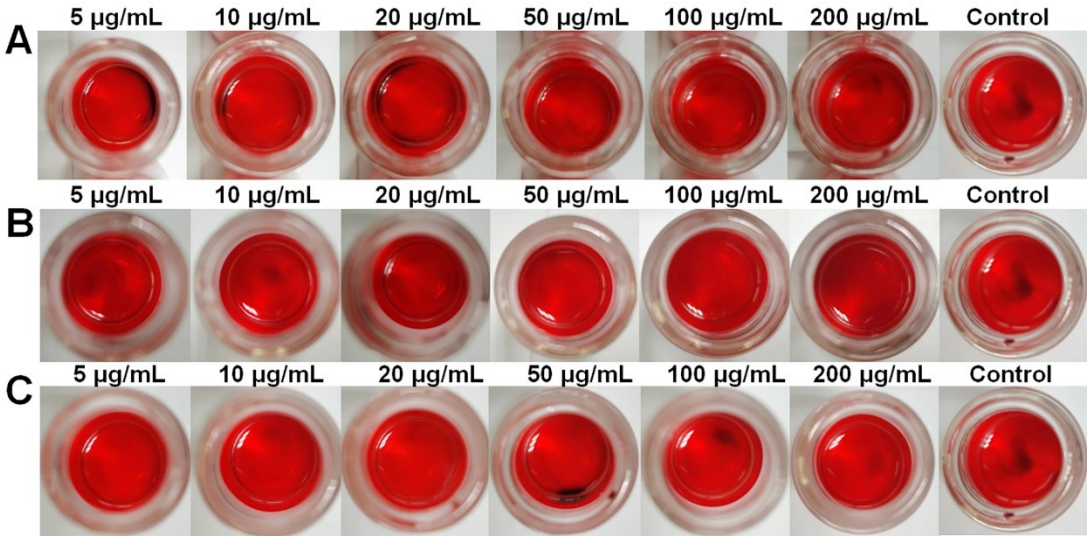

Figure S10. Anticoagulation tests for a series of the normal saline solutions of the resulting MOPF nanoparticles (A), LE@MOPF nanoparticles (B) and LE (C) with different concentrations.

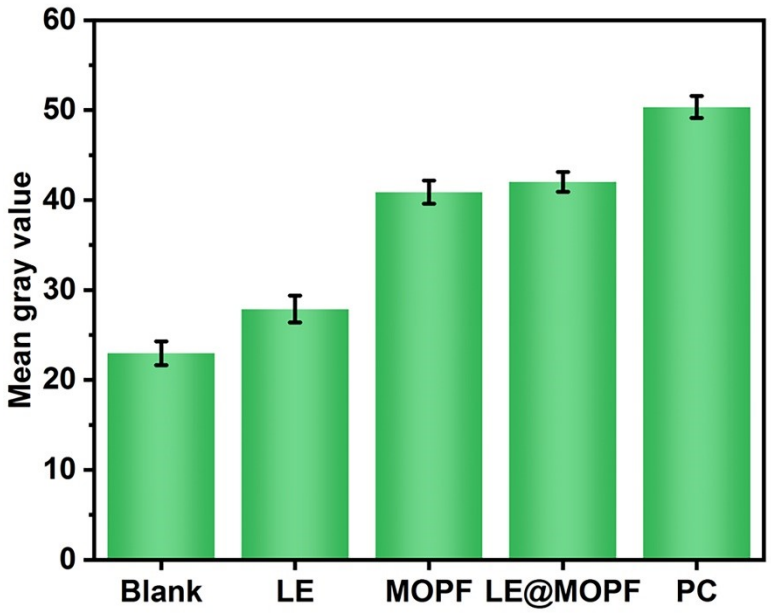

Figure S11. ROS generation levels of the DMEM solution: blank, the resulting MOPF nanoparticles (concentration: 200 μg/mL), LE@MOPF nanoparticles (concentration: 200 μg/mL), LE (concentration: 200 μg/mL) and positive control group.

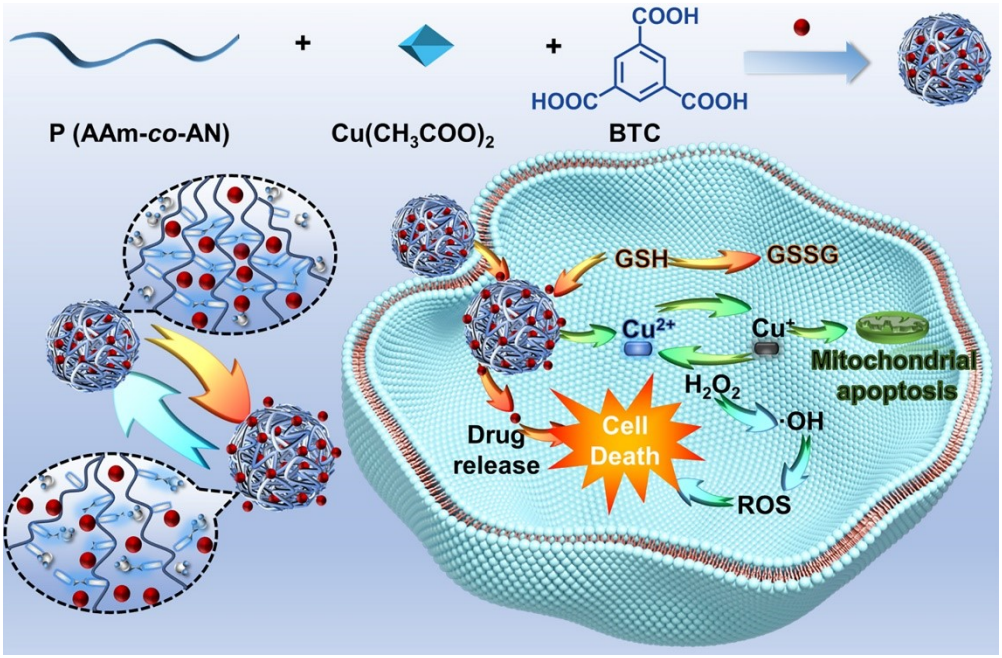
COOH
HOOC
COOH
P (AAm-co-AN)
Cu(CH3COO)2
BTC
GSH
GSSG
Cu2+
Cu+
Mitochondrial apoptosis
H2O2
·OH
Drug release
Cell Death
ROS

TOC